J Comput Aided Mol Des (2012) 26:1355–1368
DOI 10.1007/s10822-012-9619-1

New insights from molecular dynamic simulation studies of the multiple binding modes of a ligand with G-quadruplex DNA

Jin-Qiang Hou · Shuo-Bin Chen · Jia-Heng Tan · Hai-Bin Luo · Ding Li · Lian-Quan Gu · Zhi-Shu Huang

Received: 23 August 2012 / Accepted: 27 November 2012 / Published online: 13 December 2012

Abstract G-quadruplexes are higher-order DNA and RNA structures formed from guanine-rich sequences. These structures have recently emerged as a new class of potential molecular targets for anticancer drugs. An understanding of the three-dimensional interactions between small molecular ligands and their G-quadruplex targets in solution is crucial for rational drug design and the effective optimization of G-quadruplex ligands. Thus far, rational ligand design has been focused mainly on the G-quartet platform. It should be noted that small molecules can also bind to loop nucleotides, as observed in crystallography studies. Hence, it would be interesting to elucidate the mechanism underlying how ligands in distinct binding modes influence the flexibility of G-quadruplex. In the present study, based on a crystal structure analysis, the models of a tetra-substituted naphthalene diimide ligand bound to a telomeric G-quadruplex with different modes were built and simulated with a molecular dynamics simulation method. Based on a series of computational analyses, the structures, dynamics, and interactions of ligand-quadruplex complexes were studied. Our results suggest that the binding of the ligand to the loop is viable in aqueous solutions but dependent on the particular arrangement of the loop. The binding of the ligand to the loop enhances the flexibility of the G-quadruplex, while the binding of the ligand simultaneously to both the quartet and the loop diminishes its flexibility. These results add to our understanding of the effect of a ligand with different binding modes on G-quadruplex flexibility. Such an understanding will aid in the rational design of more selective and effective G-quadruplex binding ligands.

Keywords Molecular dynamics simulation · Telomeric G-quadruplex DNA · Naphthalene diimide derivative · Binding modes

Introduction

Guanine-rich single-stranded DNA or RNA can form four-stranded secondary structures called G-quadruplexes under appropriate cationic conditions [1–3]. G-quadruplexes consist of π-stacked G-quartets, square-planar platforms of four guanines connected via cyclic Hoogsteen H-bonding. DNA G-quadruplexes have been shown to form in biologically significant regions, such as human telomeres [4], oncogene promoter regions [5–7], immunoglobulin switch regions [8], ribosomal DNA [9], and certain regions of RNA. For example, human telomeric DNA consists of 5–10 kb tandem repeats of the hexanucleotide $d(TTAGGG)_n$, which has a strong propensity to form G-quadruplex structures. The formation of quadruplexes in telomeric DNA results in the inhibition of telomere elongation by telomerase in cancer cells [10, 11]. In contrast, an increasing number of proteins have been shown to preferentially bind to G-quadruplexes, and their interactions with G-quadruplexes have potential implications in a wide variety of biological phenomena including telomere maintenance [12], telomere end-capping and protection

Electronic supplementary material The online version of this article (doi:10.1007/s10822-012-9619-1) contains supplementary material, which is available to authorized users.

J.-Q. Hou · S.-B. Chen · J.-H. Tan · H.-B. Luo · D. Li · L.-Q. Gu (✉) · Z.-S. Huang (✉)
School of Pharmaceutical Sciences, Sun Yat-sen University, Guangzhou 510006, China
e-mail: cesglq@mail.sysu.edu.cn

Z.-S. Huang
e-mail: ceshzs@mail.sysu.edu.cn

[13–15], chromosome organization [8], and regulation of gene expression [16]. Therefore, the development of a small molecule to bind to G-quadruplexes and disrupt the recognition of a G-quadruplex by its binding protein has emerged as a promising anti-cancer strategy.

For rational drug design and effective G-quadruplex ligand optimization, it is important to understand the interaction between a small molecule ligand and its G-quadruplex receptor. Data from X-ray crystallography and nuclear magnetic resonance (NMR) studies have shown that small molecule ligands primarily bind the terminal G-quartets at the end of G-quadruplexes (i.e., PDB IDs 1L1H [17], 3CE5 [18], 1O0 K [19], 1NZM [20], 2JWQ [21], 2A5R [22]). Thus far, rational ligand design efforts have been mainly focused largely on the G-quartet platform [23, 24]. However, three crystal structures recently solved by Parkinson et al. (PDB IDs 2HRI [25], 3CDM [26], 3CCO [26]) have revealed that small molecules can bind to the loop nucleotides, external to the end-stacking interactions. The loops in a G-quadruplex can provide a platform for a second binding mode, which should be taken into account in structure-based drug design because the functional groups on the loops may be important for ligand recognition in different quadruplexes topologies [24]. This is important for gene targeting therapy, which is based not only on the selectivity of the small molecules for quadruplex over duplex DNA, but also on selectivity for the target quadruplex over other quadruplexes. In addition, it should be noted that most G-quadruplex-binding-proteins appear to bind the loop regions of G-quadruplexes [27], as evidenced by crystallographic structure of a quadruplex-protein complex (PDB ID: 1HUT [28]) and other biophysical studies [29]. Therefore, the development of a small molecular ligand targeting the G-quadruplex loop region may effectively block its recognition by functional proteins. However, the binding of small molecules to loop nucleotides has been observed only in crystal structures. Due to the absence of relevant NMR structures, it remains unknown whether such a loop-binding mode also exists in solution. It has been well established, through experiments and molecular dynamics (MD) simulations, that ligand binding to the G-quartet platform increases quadruplex rigidity [21, 30, 31]. However, it remains unclear whether a small molecule can be docked onto loop regions in solution states and how such docking affects the flexibility of the G-quadruplex. In addition, the mechanism by which multiple binding modes affect the flexibility of G-quadruplex remains a question of interest, as such bindings may have dual effects on G-quadruplex: (1) the binding of a ligand to the G-quartet may diminish the G-quadruplex flexibility and (2) the binding of a ligand to the loop may block the interaction between a G-quadruplex and its binding proteins.

Molecular dynamics simulations have been used as an adjunct method to support experimental results. Such simulations can aid in the avoidance of crystal packing artifacts and the elucidation of the role of solvents and ions in mediating the drug–DNA interaction. In addition, simulations provide detailed atomistic insight regarding the rearrangement state [32]. Previous MD studies on G-quadruplexes [33–37] and ligand-quadruplex interactions [38–40] demonstrated that MD is a powerful tool when evaluating experimental structures that aids in evaluating the structural dynamics of G-quadruplexes. Multiple binding modes have been observed in the crystal structure of a ligand-quadruplex complex (PDB id: 3CDM [26]), in which four tetra-substituted naphthalene diimide ligands (Fig. 1) separately stack on the G-tetrad surfaces and the same two ligands separately bind to the external TTA-loop nucleotides. The structure of 3CDM served as a good starting point for our molecular dynamics simulation study to answer several questions. (1) Can a small molecule be docked to a quadruplex loop region in solution? (2) What are the primary driving forces for such a binding mode? (3) How does a small molecule in different binding modes affect the flexibility of the G-quadruplex structure? (4) Which binding mode is favored in the design of an effective ligand for enhancing the G-quadruplex rigidity? In the present study, five models with distinct ligand-binding patterns were built based on the structure of 3CDM (Fig. 2) and simulated using a molecular dynamics method in explicit solvent. The structural role of the ligand with different binding modes, the accompanying influence on the flexibility of the G-quadruplex and their detailed interactions were elucidated through a series of computational analyses.

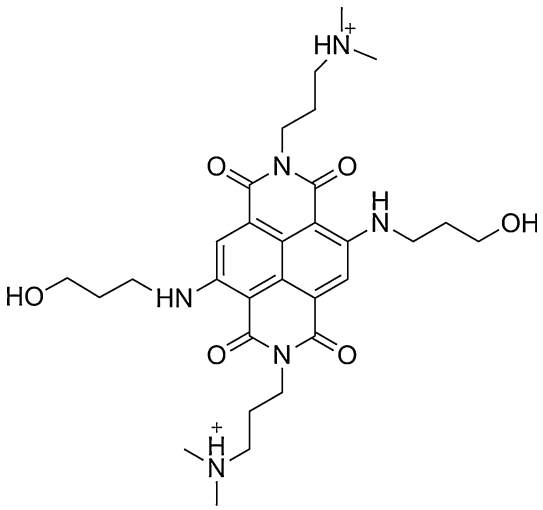

Fig. 1 The tetra-substituted naphthalene diimide ligand in a complex with G-quadruplex for the MD studies

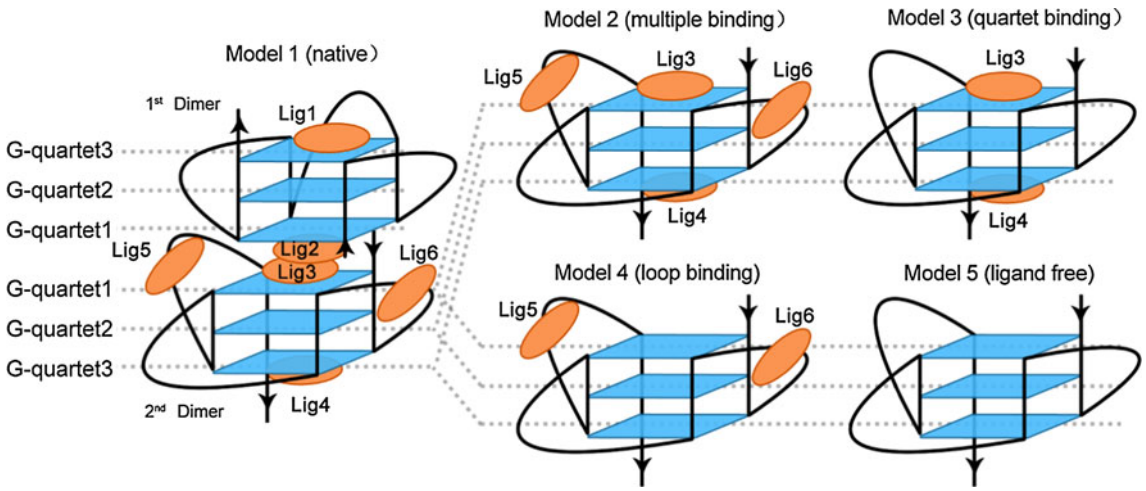

Fig. 2 Schematic representation of G-quadruplex and ligands (*orange*)

Table 1 MD simulation models

Id	Structure	Ligand net charge	Ions	Forcefield	Timescale (ns)
Model 1	Native	+2	K^+(31)	parm99	50
Model 2	Multiple-binding	+2	K^+(14)	parm99	30
Model 3	Quartet-binding	+2	K^+(18)	parm99	30
Model 4	Loop-binding	+2	K^+(18)	parm99	30
Model 5	Ligand-free	+2	K^+(22)	parm99	30
Model 1	Native	+2	K^+(31)	parmbsc0	34
Model 2	Multiple-binding	+2	K^+(14)	parmbsc0	34
Model 3	Quartet-binding	+2	K^+(18)	parmbsc0	34
Model 4	Loop-binding	+2	K^+(18)	parmbsc0	34
Model 5	Ligand-free	+2	K^+(22)	parmbsc0	30

Materials and methods

MD simulations

The partial ligand charges were computed at the HF/6–31G* level with Gaussian 03 calculation [41], followed with RESP calculation using the antechamber module of the Amber 10 program (Figure S1) [42]. Other parameters were adopted from the Generalized Amber force field (GAFF) [43].

The K^+ ions were kept in the central core of the complex as observed in the crystal structure. Every ligand-receptor system was then immersed in a truncated octahedron box of TIP3P water molecules extending up to 10 Å from the solute in each direction. Additional counter-ions (K^+) were added into the system to neutralize the negative charge on the DNA backbone. Using the Coulombic potential, the counter-ions were automatically placed into the most negative locations with the LEAP program. An Amber ff99 and parmbsc0 force field [44] was applied for the G-quadruplexes, ions, and water molecules. Simulations were performed with the SANDER program of Amber 10. All models are listed in Table 1.

The final systems were subjected to initial minimization to equilibrate the solvent and counter-ions. The G-quadruplex complex and inner ions were initially fixed with force constants of 100 kcal·mol^{-1}·Å^{-2}. Then, a 2,000-step full minimization was carried out for the entire system without restraint. The system was then slowly heated from 0 to 300 K over 100 ps at constant volume with a force constant of 50 kcal· mol^{-1}·Å^{-2} maintained for the complex and inner ions. After the heating process, a further 100-ps equilibration using 25 kcal· mol^{-1}·Å^{-2} constraint on the complex and inner ions was carried out to obtain a stable density. Afterward, the systems were then subjected to a 30–50 ns unconstrained MD simulation. All MD simulations were carried out in an NPT ensemble at 1 atm and 300 K. A residue-based cutoff of 10 Å was used for the non-bonded interactions. The H-bonds were constrained using the SHAKE algorithm [45]. Periodic boundary conditions

were applied to avoid the edge effect. The Particle Mesh Ewald (PME) method was employed to calculate long-range electrostatic interactions [46]. Temperature regulation was achieved by Langevin coupling with a collision frequency of 1.0. The time step used for the MD simulations was set to 2.0 fs, and the trajectory files were collected every 1 ps for the subsequent analysis. All trajectory analyses were performed with the Ptraj module in Amber 10 and examined visually using VMD software [47].

Binding free energy analysis

The binding free energies (ΔG_{bind}) were calculated using the MM-PBSA approach [48, 49] inside the Amber 10 program. The dielectric constants were set to 1 for the solute and to 80 for the surrounding solvent molecules. The K^+ radius was set to 2.025 Å [50]. A total of 100 snapshots were taken from the last 4-ns trajectory with an interval of 20 ps. Prior to the analysis, all counter-ions and water molecules (except for the K^+/Na^+ ions present in the central channel of the G-quadruplex) were stripped from the trajectories. For each snapshot, the free energy was calculated for each molecular species (complex, ligand, and quadruplex) using the following equation:

$$\Delta G_{bind} = G_{complex} - [G_{ligand} + G_{quadruplex}] \quad (1)$$

where $G_{complex}$, G_{ligand}, and $G_{quadruplex}$ were the free energies for the complex, quadruplex, and ligand, respectively. Each of them was estimated with the following equation [51]:

$$\Delta G_{bind} = (\Delta E_{elec} + \Delta E_{vdw} + \Delta E_{ini}) + (\Delta G_{PB} + \Delta G_{np}) - T\Delta S \quad (2)$$

where ΔE_{elec} was the Coulomb interaction, ΔE_{vdw} was the van der Waals interaction, and ΔE_{ini} was the sum of the bond, angle, and dihedral energies. In this case, $\Delta E_{ini} = 0$. ΔG_{PB} was the polar contribution to solvation, which was obtained by solving the Poisson-Boltzmann equation [52] for the MM-PBSA method. ΔG_{np} was the nonpolar solvation term. $-T\Delta S$ was the entropy term. The nonpolar solvation term was computed in (3):

$$\Delta G_{np} = \gamma \Delta SASA + b \quad (3)$$

where γ was the surface tension that was set to 0.0072 kcal/(mol Å^2), and b was a constant that was set to 0 [53]. SASA is the solvent-accessible surface area (Å^2) that was estimated using the MOLSURF algorithm. The solvent probe radius was set to 1.4 Å to define the dielectric boundary around the molecular surface.

The calculation for the entropic contribution was performed with the NMODE module, which computes vibrational, rotational, and translational entropies. A total of 100 snapshots were collected from the last 2 ns of the trajectory at 20 ps intervals. Each snapshot was minimized using the conjugate gradient method for 10,000 steps with a distance-dependent dielectric constant of 4 interatomic distances. The terminating criterion for minimization was set to 0.01 kJ/mol•Å gradient RMS.

Hydration analysis

Water density was calculated by RMS coordinate fitting over all DNA atoms at 2 ps intervals into 0.5 Å^3 grids from the last 2-ns trajectories. The value of each grid element represents the number of times the coordinates of water oxygen were within the 0.5 Å^3. These grids were then contoured using UCSF Chimera. The expected number of waters per grid element is 4.18 for 1,000 frames, representing the bulk water density. In the presented hydration image, the contouring of the water density was performed at 12.0 hits per 0.5 Å^3, which is approximately three-fold the expected bulk water density. The contours of the water oxygen density are displayed using Chimera [54].

Principal components analysis

It is helpful to reduce the dimensionality of the data obtained from MD simulations when determining the principal components of motion. Principal components analysis (PCA) is a powerful method that reduces data dimensionality by performing a covariance analysis between factors [37, 55, 56]. Briefly the method was performed as explained in the following. First, each frame of the trajectory was fit to the starting structure to eliminate translational and rotational motions and to isolate only the internal motions of the system. The atoms are identified in the structure moving together through the generation of a covariance 3 N × 3 N matrix. Then, the covariance matrix was diagonalized to obtain a set of eigenvectors and corresponding eigenvalues, which represented the directions of motion and the amplitude of motion along each eigenvector, respectively. Herein, PCA was carried out using PCAZIP software [57] on backbone atoms. The last 6-ns trajectories (3,000 frames) were extracted using the PTRAJ program for the analysis.Graphic models were prepared using PyMOL (version 0.9) [58], Discovery Studio (Accelrys, San Diego, CA), or Xmgrace (http://plasma-gate.weizmann.ac.il/Grace/).

Results

Model construction

As mentioned above, three crystal structures solved by Parkinson et al. [26] revealed that small molecule can bind

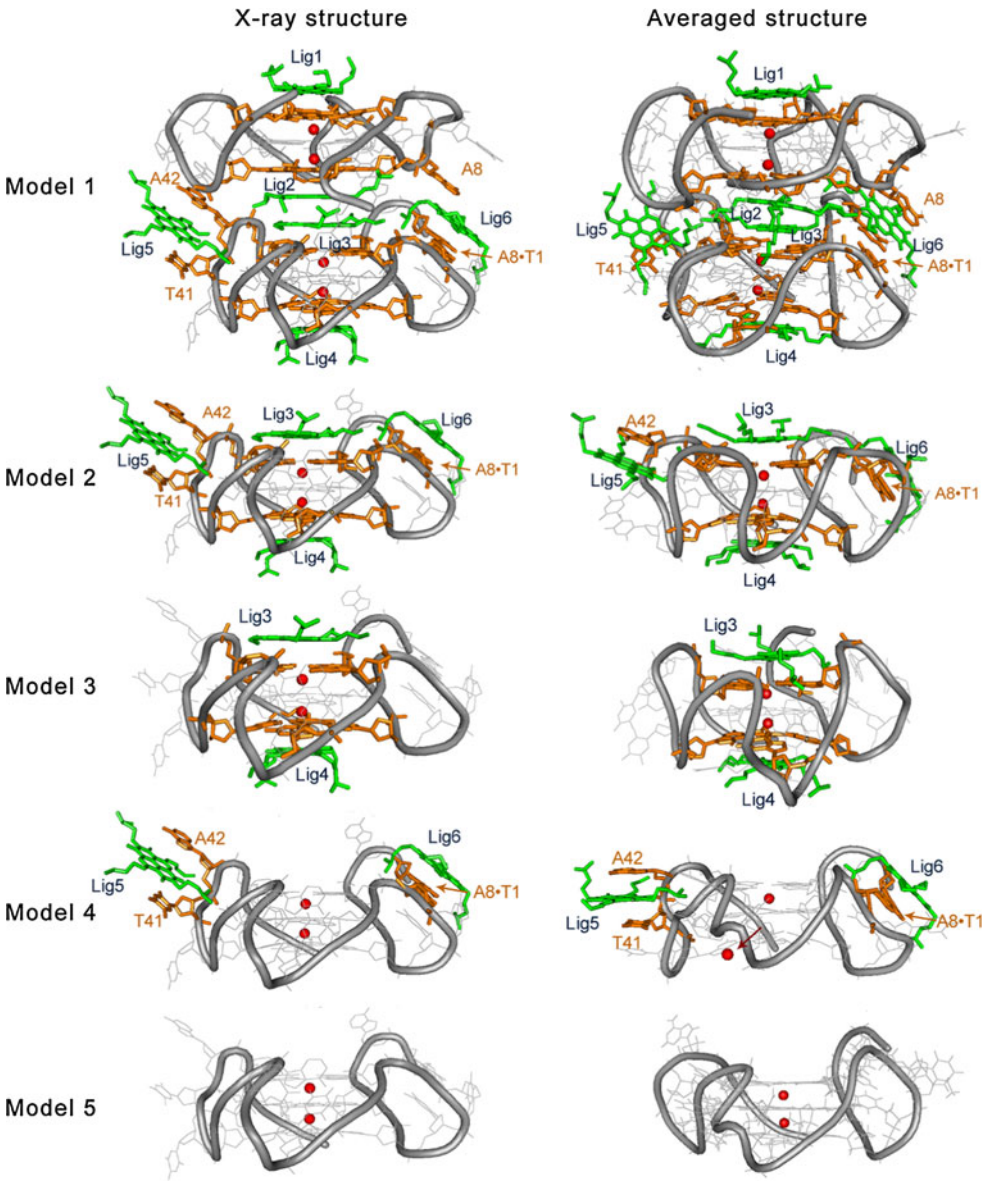

Fig. 3 Comparison of X-ray structure and simulated structure in the parm99 force field. Ligands are shown as *green sticks*. Residues stacking with the ligands are shown as *orange sticks*. The K^+ ions are shown as *red spheres*

to loop nucleotides. Among these complexes, 3CDM exhibits unique ligand binding patterns, in which four ligands separately stack on G-tetrad surfaces and two ligands separately bind to the external TTA-loop nucleotides. Therefore, by dividing the multiple binding modes into purely quartet-binding and loop-binding modes, the impact of quadruplex ligand binding with these two distinct binding modes on the flexibility of G-quadruplex structure could be investigated. As shown in Fig. 2, five models were built based on the crystal structure. Model 1 is the native ligand-quadruplex complex. Model 2 is a multiple-binding structure, where four ligands are simultaneously bound to the G-quartets and the loops. Model 3 is a G-quartet-binding structure, where two ligands are separately bound to the two ends of the G-quadruplex. Model 4 is a loop-binding structure, where two ligands are separately bound to the G-quadruplex loops. A comparison of MD studies examining Models 2-4 aided in elucidation of how ligands in different binding modes affect the flexibility of G-quadruplex structures. Model 5 is a ligand-free model that was used as a reference structure.

Comparison of the X-ray and simulated structures

To confirm some general considerations, a comparison of the X-ray and averaged structures for all models was performed (Fig. 3 and Figure S2). The averaged structures were obtained by averaging 100 MD simulation snapshots, which were taken from the last 4 ns on the MD trajectories with an interval of 20 ps. K^+ ions play an important role in stabilizing the G-quadruplex structure. In the starting structure, K^+ ions were located in the ion channel. In the

Table 2 H-Bond Map of the X-ray complex and simulated complex

	Donor	Acceptor	Model	Donor	Acceptor	Occupancy (%)
Crystal structure	Lig2@O2	WAT	Model 1	G37@O2P	Lig2@H85 Lig2@N5	99.95
	WAT	Lig2@H86 Lig2@N4		G14@O2P	Lig3@H86 Lig3@N4	99.80
	Lig2@O6	WAT		A24@O2P	Lig6@H86 Lig6@N4	99.50
	Lig3@N4	Lig2@H1 Lig2@O6		G14@O2P	Lig2@H1 Lig2@O6	98.95
	G31@O2P	Lig3@H1 Lig3@O6		Lig6@O1	T29@H3 T29@N3	97.45
	T41@O2P	Lig5@H86 Lig5@N4		G32@O1P	Lig3@H85 Lig3@N5	95.65
	A42@O4	Lig5@H42 Lig5@O5	Model 2	Lig6@O1	T7@H3 T7@N3	53.47
	T23@O2	Lig6@H86 Lig6@N4	Model 3	A2@O2P	Lig3@H86 Lig3@N4	73.61
	Lig6@O4	WAT		T1@O2	Lig3@H1 Lig3@O6	58.67
	Lig6@O3	WAT	Model 4	G17@O1P	Lig5@H86 Lig5@N4	98.90
	WAT	Lig6@H2 Lig6@O5		T7@O1P	Lig6@H85 Lig6@N5	77.91
	WAT	Lig6@H1 Lig6@O6				

The listed donor and acceptor pairs satisfy the criteria for H-bonding over 40.0 % of the last 4 ns of the simulations

case of parm99 force field, the averaged structure in Fig. 3 indicates that K^+ ions were well preserved in all models during the simulations, expect for Model 4. In Model 4, the K^+ ion between quartet 2 and quartet 3 escaped from the ion channel, and consequently, the G-quartet 3 became disordered. Interestingly, in the case of parmbsc0 force field, the K^+ ion between quartet 1 and quartet 2 escaped from the ion channel in Model 4 (Figure S2).

In the X-ray structure, Lig1-4 stack on the G-quartet surface. Lig5 is intercalated between the A42 and T41 from a single loop. Lig6 is intercalated between A8 of the 1st dimer and a planar platform formed from a Watson–Crick A8·T1 base pair of the 2nd dimer. In the simulated structures, not all of these interactions were well preserved, as shown in Fig. 3 and Figure S2. For Model 1, the loop-binding ligand in the Lig5 position lost its π–π stacking interaction with A42 in parm99, and the loop-binding ligand in the Lig6 position lost its π–π stacking interaction with A8 in parmbsc0. For Model 2, the ligand at the same position lost its π–π stacking interaction with T41 in both parm99 and parmbsc0. This implies that the ligand binding to the loop regions is dynamic in aqueous solution.

To compare H-bond mapping between the crystal structure and the simulated structures, the H-bonds were calculated from the last 4-ns trajectories. The formation of a H-bond was defined in terms of distance and orientation. An interaction was considered to be a H-bond if the distance between the hydrogen donor and acceptor was less than 3.5 Å and the angle was greater than 120.0°. The H-bonding data in the parm99 force field are listed in Table 2. The map of the H-bonds between the ligand and quadruplex changed dramatically. To our surprise, the initially formed H-bonds all disappeared during simulation.

Structural flexibility of the G-quadruplex

G-Quartet flexibility

RMSD analyses To measure the flexibilities of G-quartets during the MD simulations, the root mean-square deviation (RMSD) values for the heavy atoms in the G-quartets were monitored for all MD trajectories and compared with the corresponding crystal structure as shown in Fig. 4 and Figure S3. The RMSD curves in Fig. 4 and Figure S3 demonstrate that the G-quartets are very rigid except for Model 4. In Model 4, a shift of the RMSD value at approximately 14 ns from approximately 0.5–1.0 Å was observed in the parm99 force field. The time-evolution of the distance between two K^+ ions in the ion channel revealed that a K^+ ion escaped from the internal ion channel at 14 ns (Figure S4). Consequently, a disruption tendency was appreciable in the G-quartet 3 layer. However, the other two G-quartet layers successfully survived for the duration of the simulation. In parmbsc0 force field, a jump of the RMSD value at approximately 9 and 22 ns were observed in Model 4 (Figure S3) and the time-evolution of the distance between two K^+ ions in the ion channel revealed that a K^+ ion escaped from the internal ion channel at 30 ns (Figure S5). This result implies that ligand binding to the loops has a positive impact on the flexibility of G-quartets.

The primary forces promoting G-quadruplex stability are the G-quartets held by eight Hoogsteen H-bonds (N2–H21…N7 and N1–H1…O6) [59–61]. To study the influence of the ligands with different binding modes on the G-quartet flexibilityin detail, the H-bond occupancies (fractions of time that the H-bonds are formed during simulation) of the G-quartets were calculated from the last 4 ns-trajectories in the parm99 force field, as shown in

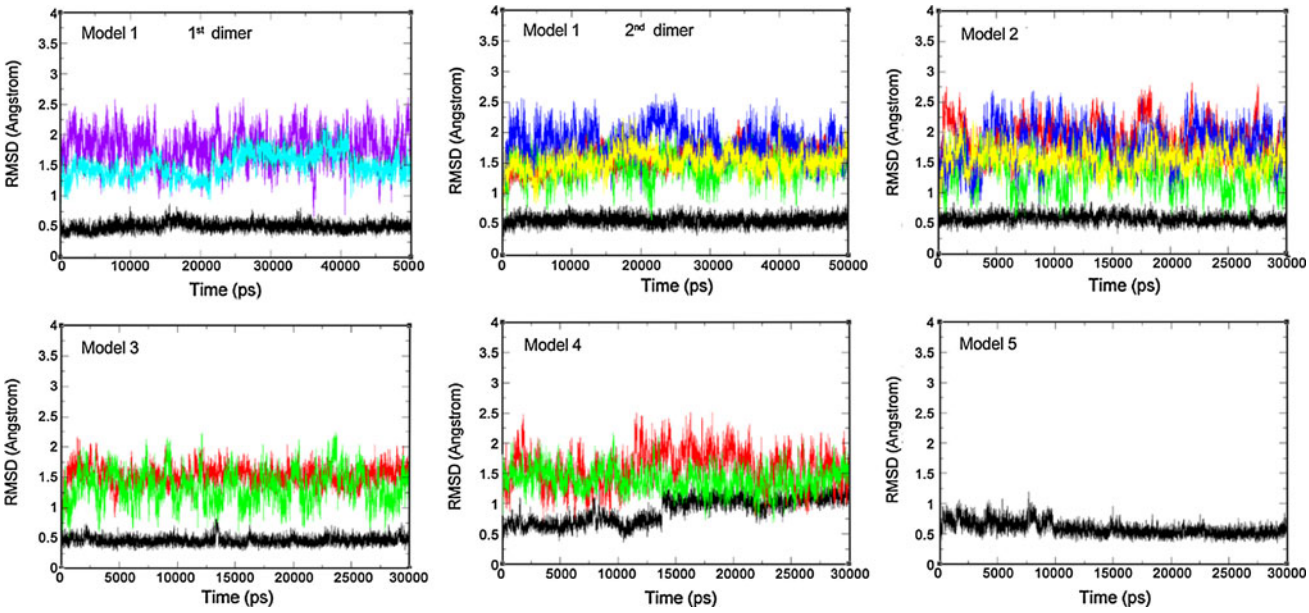

Fig. 4 Time dependence of the RMSD of the G-quartet heavy atoms and all ligand atoms in the parm99 force field. G-quartet heavy atoms are shown in *black*; Lig1, Lig2, Lig3, Lig4, Lig5 and Lig6 are shown in *purple*, *cyan*, *red*, *green*, *blue*, *yellow*, respectively

Fig. 5. Table 3 and Table S1 list the average occupancy of the eight H-bonds for each G-quartet in the parm99 and parmbsc0 force fields. Model 1, Model 2, and Model 3 accommodated quartet-binding ligands. For these models, the observed average H-bond occupancies indicated that the outer G-quartets (G-quartet 1 and G-quartet 3) are more stable compared to the inner G-quartets (G-quartet 2). This result is consistent with our previous MD simulation results for quartet-binding ligands and G-quadruplex complexes [62].

In the case of parm99 force field, the average H-bond occupancies of G-quartet 3 in Model 4 are very low (55.96 %), indicating the disruption of some Hoogsteen H-bonds in the G-quartet 3 layer in this model. The average H-bond occupancy of all G-quartets within this structure is 84.95 %, which is lower than that of Model 5 (98.01 %). These results again suggest that ligand binding to the loop enhances the G-quartet flexibility. Surprisingly, for Model 2, the average H-bond occupancy of all G-quartets is 99.18 %, which is highlighted when compared with the other models. This suggests that ligands simultaneously binding to the G-quartet and the loops diminish the G-quartet flexibility. The results from the simulations in the parmbsc0 force field are similar (Table S1), supporting the conclusion that ligand binding to the loop enhances the G-quartet flexibility, while ligands simultaneously binding to the G-quartet and the loops diminish the G-quartet flexibility. It should be noted that, after one K^+ ion escaped, the G-quartets were maintained better in parmbsc0 force field than in parm99 force field.

Backbone stability

Principal component analysis The stability of the G-quadruplex may be dependent on both the G-quartets and backbones. To further identify the magnitude of backbone motions in the models, a principal components analysis (PCA) was applied to the backbone atoms of all systems for the last 6 ns simulations in the parm99 force field. The eigenvalues representing the magnitude of the motions of the first four eigenvectors for all simulation systems were calculated as shown in Table 4 and Figure S6. As the eigenvalue decreases, the flexibility of the G-quadruplex backbone also decreases.

The ranking order of eigenvalues for all models was as follows: Model 5 > Model 4 > Model 3 ≥ Model 2 > Model 1. The eigenvalues for all complexes were smaller than that of the ligand-free model, suggesting that ligand binding to any site can make the G-quadruplex backbone more rigid. By comparing the eigenvalues of Model 3 with those of Model 4, we can conclude that ligand binding to the G-quartet is more effective for backbone rigidity than loop binding. For the quartet-binding mode, the rigidity effect mainly arises from electrostatic and/or H-bond interactions between the protonated tertiary amine among the ligand side chains and the quadruplex backbone. For the loop-binding mode, ligand binding to the loop nucleotides decreased their wobbling motions by stacking onto them, thus diminished the backbone flexibility. For Model 2, the eigenvalues were lower than those of Model 3, Model 4, and Model 5, suggesting that the ligand with multiple-binding modes

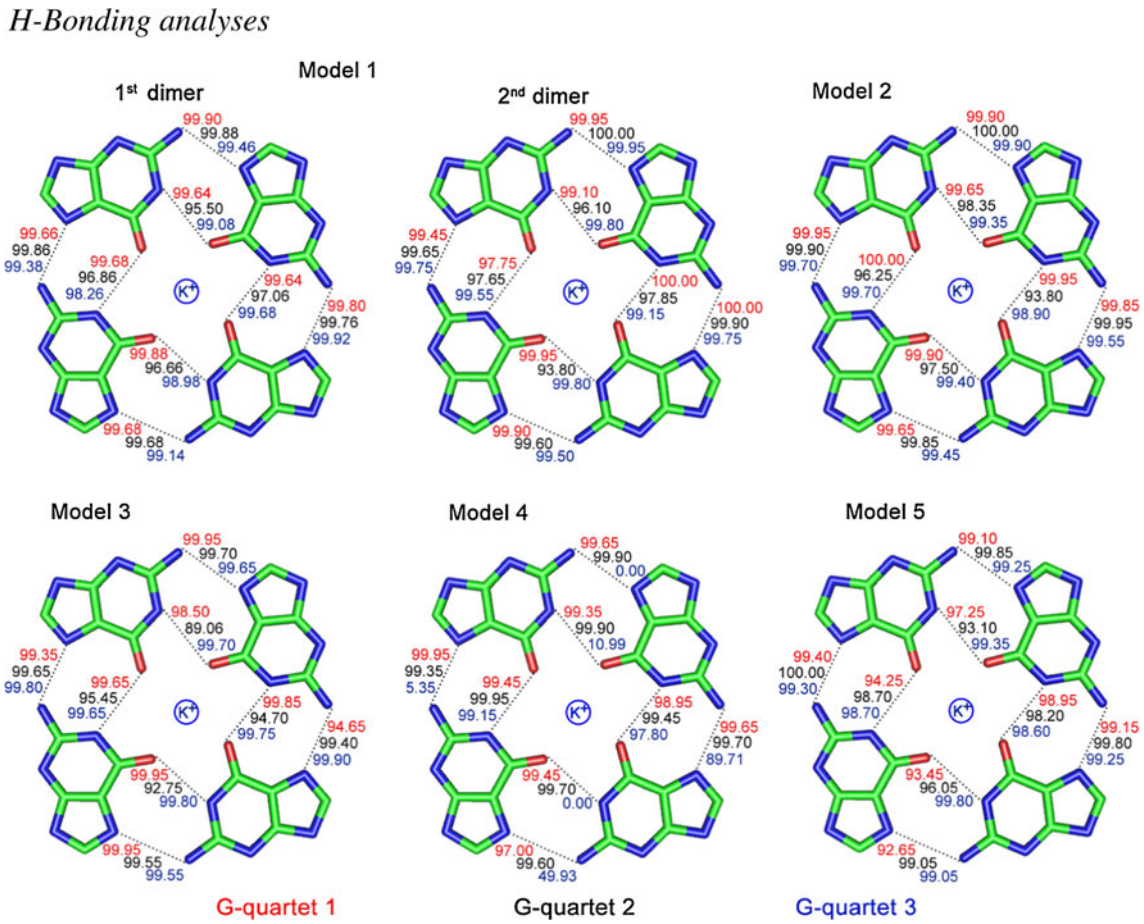

Fig. 5 H-bond occupancies within every G-quartet during the MD simulations in the parm99 force field. Occupancy is provided as a percentage of the investigated time period

Table 3 Average occupancy (%) of eight H-bonds in each G-quartet calculated from the last 4-ns trajectories in the parm99 force field

	Model 1		Model 2	Model 3	Model 4	Model 5
	1st dimer	2nd dimer				
G-quartet 1	99.74	99.51	99.86	98.98	99.18	96.78
G-quartet 2	98.16	98.07	98.20	96.28	99.69	98.09
G-quartet 3	99.24	99.66	99.49	99.73	55.96	99.16
Average	99.04	99.08	99.18	98.33	84.95	98.01

Table 4 Eigenvalues ($Å^2$) of the First Four Eigenvectors for all models in the parm99 force field

	Model 1		Model 2	Model 3	Model 4	Model 5
	1st dimer	2nd dimer				
Eigenvector1	13.4	9.7	15.3	15.0	29.7	37.1
Eigenvector2	5.7	6.5	10.2	12.4	13.4	23.4
Eigenvector3	5.4	5.2	7.3	7.5	11.8	16.5
Eigenvector4	4.2	3.8	6.2	5.1	10.1	13.5

diminishes the quadruplex backbone flexibility effectively. The lowest eigenvalues were observed in Model 1, suggesting that in addition to ligand binding, quadruplex dimer formation also contributes to backbone rigidity.

Hydration patterns

The aqueous saline environment is known to play an important role in the stability of DNA conformations and configurations. It is clear that water is an integral part of nucleic acid structure [63]. Recently, Trent et al. [64] reported that hydration is a major determinant of G-quadruplex stability and the conformation of the human telomere. Chalikian et al. [65] have reported that the folding transitions of G-rich sequences are accompanied by a release of 103 ± 44 water molecules from hydration shells to the bulk of the structure. These investigations have highlighted the importance of hydration in G-quadruplex structure and flexibility. Herein, to provide a general picture of the overall hydration situation in the simulations, and to characterize the distinction among the different models, water density around the structure was computed

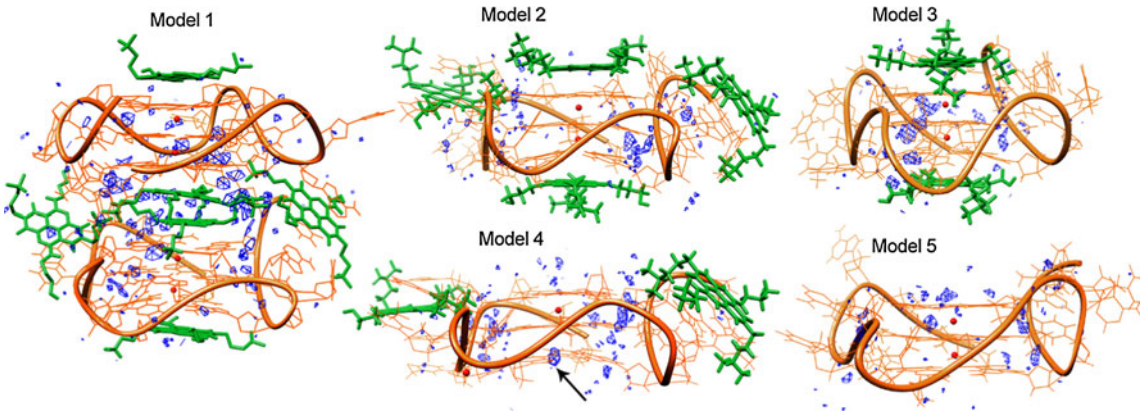

Fig. 6 The averaged structures and their hydration sites over the last 2-ns trajectories. The contours of the water oxygen density represent approximately threefold bulk water density

for the last 1-ns trajectories in the parm99 force field. As depicted in Fig. 6, the average structures displayed approximately threefold bulk water density around themselves, revealing highly occupied hydration sites. The most distinguishable hydration sites were localized inside the grooves for all models. These results are in agreement with hydration patterns observed in the crystal structures [26] and previous MD studies of $d(TG_4T)_4$ quadruplexes [66]. However, the hydration sites observed in the grooves of different models were not identical. It is possible that the ligand binding to the quadruplex rearranged the loop conformation, which changed its access to H-bond donors and acceptors, thus altering the hydration networks. Specifically, for Model 4, due to the escape of K^+ ion from the ion channel, a clear hydration site within the G-quartet 3 was formed in the averaged structure, capping the ion channel entrances (Fig. 6, indicated by arrow). In addition, sparse and small hydration sites on the exposed G-quartet were also observed in Model 4 and Model 5. However, little or no hydration sites on the G-quartet were observed in the models where G-quartets were occupied by hydrophobic core of the ligand. This phenomenon, although not significant, may imply that aromatic ligand binding to the G-quartet could facilitate the formation of a quadruplex dimer or even multimer by stacking, as observed in the crystal structure. For Model 1, a high number of hydration sites around the joint area between the two quadruplex monomer were observed. These sites may aid in stabilize the quadruplex dimer in solution.

Interaction of ligands with G-quadruplexes

Dynamic properties of ligand binding to G-quadruplexes

To investigate the conformational changes of the ligand, mass-weighted RMSDs (mwRMSDs) between the simulated ligand conformations in the parm99 force field and the initial conformation were calculated (Fig. 4). The large mwRMSD fluctuations observed in all models can be attributed to the side chains at the ligand cyclic scaffold. As listed in Table 5, the average mwRMSD values for the ligands are between 1.33 and 1.86 Å. When the side chains are discounted, the average RMSD values are between 0.11 and 0.14 Å. These results indicate that, in any binding mode, the ligand's side chains are more flexible than its cyclic scaffolds. These results also suggest that either the quartet-binding or loop-binding ligands are stable in the aqueous solution without a significant shift in position.

Table 5 The average mass-weighted RMSD Values of the ligands of all atoms calculated from the MD simulations in the parm99 force field

	Model 1	Model 2	Model 3	Model 4
Lig1	1.80 (0.12)			
Lig2	1.49 (0.11)			
Lig3	1.59 (0.10)	1.88 (0.14)	1.52 (0.12)	
Lig4	1.45 (0.10)	1.33 (0.10)	1.33 (0.12)	
Lig5	1.86 (0.12)	1.79 (0.13)		1.58 (0.12)
Lig6	1.53 (0.12)	1.55 (0.13)		1.38 (0.11)

Numbers in parentheses are the average RMSD values for the cyclic carbons in ligands

To better understand the fluctuations of the conformation and orientation of ligands, forty conformation snapshots were taken from the last 4-ns trajectories in the parm99 force field, with an interval of 50 ps. These structures were superposed and depicted in Fig. 7. These conformation snapshots indicate that the ligands could be docked to either the G-quartet or the loop nucleotides in each model. However, the degrees of their conformational fluctuations were different. For Model 1, the forty ligand conformation snapshots in the Lig2 and Lig3 sites were superposed very well, indicating that the binding of this ligand at both sites was very stable, whereas the forty

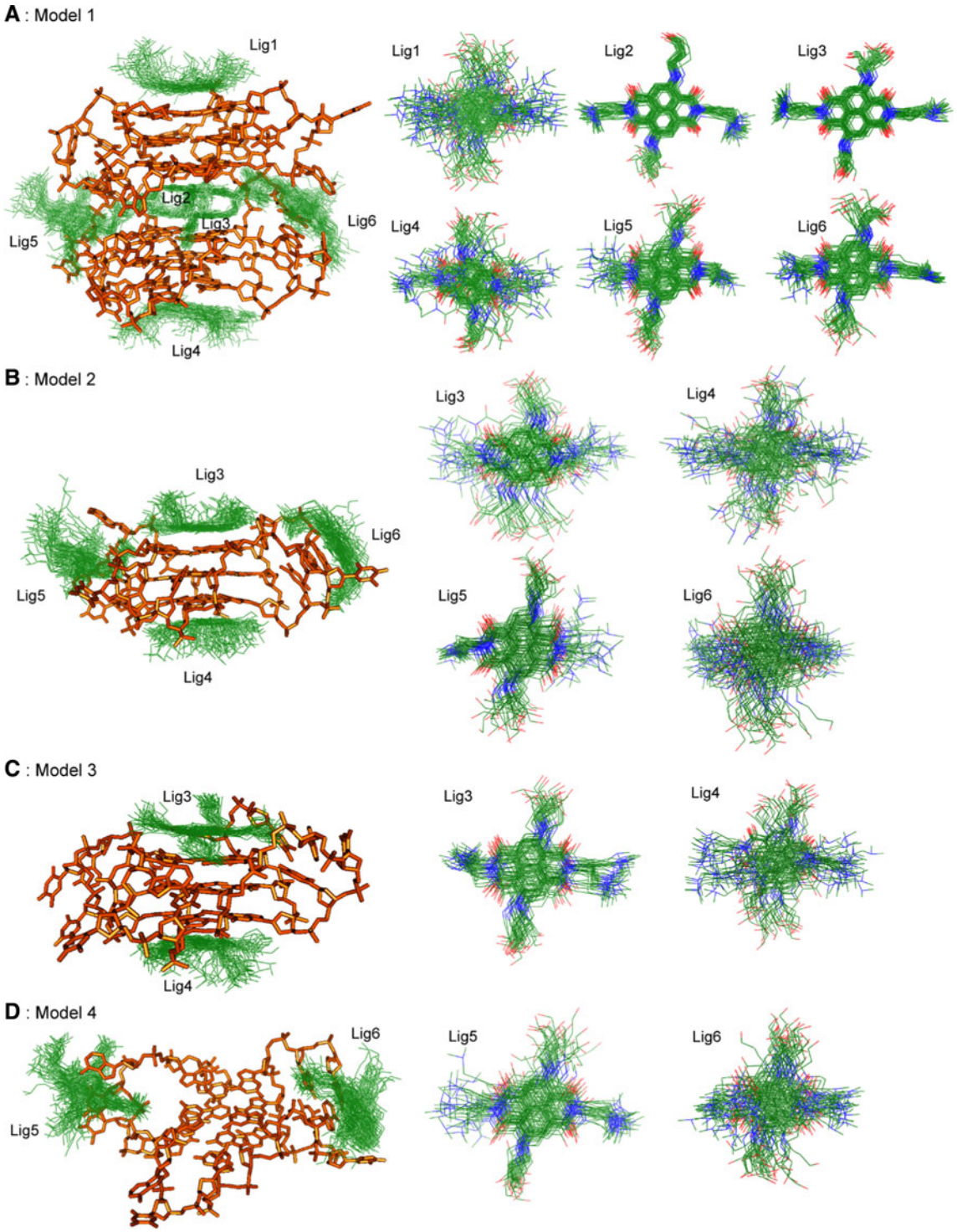

Fig. 7 Dynamics snapshots of the ligands taken from the last 4-ns trajectories

conformation snapshots indicated the worst superposition at the Lig1 and Lig4 sites indicating that ligands binding to those sites experienced large deviations. The Lig2 and Lig3 pockets were deeper between the two G-quadruplexes, while the Lig1 and Lig4 sites were exposed to the solvent. The ligands binding in the Lig5 and Lig6 sites were also stable, with comparable degree of fluctuations. The ligands binding to the quartet and binding to the loop in the other models demonstrated similar results. Importantly, quartet-binding ligands had only in-plane motions due to the stacking interaction with G-quartets, the most rigid part of a G-quadruplex. For loop-binding ligands, in addition to

Table 6 Computed binding free energies for ligand-quadruplex complexes in the parm99 force field (kcal/mol)

	Model 1					
	Lig1	Lig2	Lig3	Lig4	Lig5	Lig6
ΔE_{elec}	−1,213.1	−1,708.3	−1,723.7	−1,274.7	−1,487.0	−1,503.2
ΔE_{vdw}	−45.2	−62.5	−65.3	−48.4	−49.0	−60.0
ΔE_{ini}	0.0	0.0	0.0	0.0	0.0	0.0
ΔG_{mm}	−1,258.3	−1,770.8	−1,788.9	−1,323.1	−1,536.0	−1,563.1
ΔG_{np}	−4.2	−7.5	−8.2	−4.9	−6.5	−7.5
ΔG_{PB}	1,219.3	1,709.8	1,728.1	1,280.4	1,496.2	1,508.4
ΔG_{solv}	1,215.1	1,702.3	1,720.0	1,275.5	1,489.7	1,500.8
$\Delta G_{elec,tot}$	6.1	1.6	4.4	5.7	9.2	5.2
ΔG_{tot}	−43.2	−68.5	−69.0	−47.6	−46.3	−62.3
$-T\Delta S$	−27.0	−23.2	−25.7	−28.0	−24.0	−25.7
ΔG_{bind}	−16.5	−45.3	−43.3	−19.6	−22.2	−36.6
	Model 2				Model 3		Model 4	
	Lig3	Lig4	Lig5	Lig6	Lig3	Lig4	Lig5	Lig6
ΔE_{elec}	−828.8	−824.0	−791.1	−838.4	−1,012.9	−842.9	−837.4	−887.8
ΔE_{vdw}	−49.3	−48.3	−45.3	−43.8	−64.8	−47.9	−41.1	−41.6
ΔE_{ini}	0.0	0.0	0.0	0.0	0.0	0.0	0.0	0.0
ΔG_{mm}	−878.1	−872.2	−836.5	−882.2	−1,077.6	−890.8	−878.5	−929.4
ΔG_{np}	−5.1	−4.7	−5.7	−5.3	−6.9	−4.6	−5.2	−5.4
ΔG_{PB}	841.9	836.6	807.0	842.0	1,036.1	854.3	846.0	901.5
ΔG_{solv}	836.8	831.9	801.4	836.8	1,029.2	849.7	840.8	896.2
$\Delta G_{elec,tot}$	13.1	12.6	15.9	3.6	23.3	11.4	8.6	13.7
ΔG_{tot}	−41.3	−40.3	−35.1	−45.4	−48.5	−41.1	−37.7	−33.2
$-T\Delta S$	−27.7	−28.7	−23.6	−26.0	−28.8	−26.3	−23.3	−27.3
ΔG_{bind}	−13.6	−11.7	−11.5	−19.4	−19.6	−14.6	−14.4	−5.9

ΔE_{elec} is the electrostatic interaction calculated with the MM force field. ΔE_{vdw} is the van der Waals contribution from MM. ΔE_{ini} is the internal energy. ΔE_{mm} is the total molecular-mechanical energy ($\Delta E_{ele} + \Delta E_{vdw} + \Delta E_{ini}$). ΔG_{np} is the nonpolar contribution to the solvation energy. ΔG_{PB} is the electrostatic contribution to the solvation energy calculated by the PB approach. ΔG_{solv} is the total solvation energy ($\Delta G_{np} + \Delta G_{PB}$). $\Delta G_{elec,tot}$ is the total electrostatic energy ($\Delta G_{elec} + \Delta G_{PB}$). ΔG_{tot} is the total energy without solute entropic contribution ($\Delta E_{mm} + \Delta G_{solv}$). $-T\Delta S$ is solute entropic contribution, where T = temperature and S = sum of translational, rotational, and vibrational entropies. ΔG_{bind} is the total energy with solute entropic contribution ($\Delta G_{tot} - T\Delta S$)

the in-plane motions, up-and-down motions were apparent. This is because the G-quadruplex loop nucleotides are flexible in aqueous solution and loop-binding ligands need to be mobile to accommodate the wobbling loop nucleotides. Overall, these results suggested that small molecules can be docked to either the G-quartet or the loop in all models with comparable degree of fluctuations, and the binding of the ligands at the Lig2 and Lig3 sites in Model 1 is the most stable.

Energetic analyses of the ligand-quadruplex complexes

The MM-PBSA (Molecular Mechanic/Poisson-Boltzmann Surface Area) method was applied to compute the binding free energies for all complexes in the parm99 force field. The individual energy components and absolute free energies are listed in Table 6. Our aim was to understand the relative binding free energy order of the ligands in different binding sites, thus allowing a better understanding of the preferential ligand site and their driving forces. The binding free energies for all the models ranged from −5.9 to −45.3 kcal·mol^{-1}. MM-PBSA usually reproduces the binding free energy trends but tends to overestimate the absolute values of free energy differences [67, 68]. For all models, the electrostatic energy (ΔE_{elec}), the van der Waals energy (ΔE_{vdw}) and the nonpolar solvation energy (ΔE_{np}) presented favorable contributions to the total binding free energy. These results suggest that electrostatic energy, van der Waals forces, and polar solvation energy are the primary driving forces for ligand binding to the G-quadruplex.

However, the solvent electrostatic energy (ΔE_{PB}) and entropic effect ($T\Delta S$) presented unfavorable contributions to all complexes.

For Model 1, the ligand's binding free energies in all sites were more negative than those from the other artificial models, indicating that either quartet-binding or loop-binding ligands in this model were the most stable. The binding free energies for Lig2- and Lig3-site ligands were extremely negative because these pockets were deeper between the two G-quadruplexes, and the ligands interacted with both G-quadruplexes. For Model 3, the binding free energies for Lig3- and Lig4-site ligands were -19.6 and -14.6 kcal·mol^{-1}, respectively, which were more negative than those calculated for Model 2. This suggests that the binding of the ligand to the G-quartet is more stable in the purely quartet-binding mode than in the multiple-binding mode. This may be because the ligands binding to the loops induces the rearrangement of the loops and thus influences the interaction between the side-chains of the quartet-binding ligand and loops/grooves of the G-quadruplex.

Overall, the binding free energy analyses suggest that the binding of the ligand to the G-quartet is always stable. The binding of the ligand on the loop is not always stable and depends on the particular arrangement of the loop, as suggested by Model 4. The G-quartet ligand binding could influence the loop binding. Similarly, ligand loop binding could also influence ligand G-quartet binding.

Discussion

Ligand G-quartet binding was always stable in all simulations, as elucidated from structural analyses and binding free energy calculations. Therefore, the G-quartet surface might be the preferential site for ligand binding. These results are consistent with a wide range of experimental results [23]. However, ligand loop binding was not inherently stable, which was significantly dependent on the particular arrangement of the loops. Nevertheless, the results suggest that the binding of the ligand to the loop is viable in aqueous solution and is not due to crystal packing effects. Recently, Phan et al. [69] reported using an NMR method to detect the formation of a duplex within the long propeller loop upon the addition of a complementary strand, although the main driving force of the formation was Watson–Crick H-bonding rather than electrostatic and van der Waals interactions, as observed in the present study. These results suggest that the loop could serve as a new recognition motif and should be seriously taken into account for structure-based drug design. However, the design of ligand loop binding is a challenge, as it relies on the particular arrangement of loop residues. Recently, a structural study of two crystal structures of tetra-substituted naphthalene diimide compounds with the identical sequence d(AG_3[TTAG3]$_3$) was performed. These compounds also promote parallel-stranded quadruplex topology, with exclusive binding to the 3′ surface of each quadruplex with 1:1 stoichiometry. This is likely a consequence of the positively charged N-methyl-piperazine side-chains, major determinants of binding site affinity and groove interactions [70].

The flexibility of the G-quadruplex could be assessed by considering the flexibility of both the G-quartet and the backbone. The results from G-quartet RMSD, H-bonding suggested that ligand loop binding decreased G-quartet rigidity, while combined ligand loop and G-quartet binding enhanced the G-quartet rigidity. However, the principal component analysis indicated that the ligand loop binding also increased backbone rigidity. As the G-quartets and the central ion are the key structural elements for a G-quadruplex [67], and ion escape and G-quartet 3 distortion were directly observed in the loop-binding model, which suggests that ligand loop binding had a negative impact on G-quadruplex rigidity. The backbone flexibility trend is consistent with the G-quartet flexibility trend in the other models. Therefore, the overall results suggest that the binding of the ligand to both the loop and the G-quartet enhanced the G-quadruplex rigidity. This is important for the development of more effective G-quadruplex ligands, as such a binding pattern may also block the interaction between a G-quadruplex and its binding proteins.

Acknowledgments We thank the Natural Science Foundation of China (Grants U0832005, 90813011, 21172272), the International S&T Cooperation Program of China (2010DFA34630), and the Science Foundation of Guangzhou (2009A1-E011-6) for their financial support of this study. The water oxygen density contours were produced using the UCSF Chimera package from the Resource for Biocomputing, Visualization, and Informatics at the University of California, San Francisco (supported by NIH P41 RR001081).

References

1. Burge S, Parkinson GN, Hazel P, Todd AK, Neidle S (2006) Quadruplex DNA: sequence, topology and structure. Nucleic Acids Res 34:5402–5415
2. Dai J, Carver M, Yang D (2008) Polymorphism of human telomeric quadruplex structures. Biochimie 90:1172–1183
3. Davis JT (2004) G-quartets 40 years later: from 5′-GMP to molecular biology and supramolecular chemistry. Angew Chem Int Ed Engl 43:668–698
4. Henderson E, Hardin CC, Walk SK, Tinoco I Jr, Blackburn EH (1987) Telomeric DNA oligonucleotides form novel intramolecular structures containing guanine–guanine base pairs. Cell 51:899–908
5. Dexheimer TS, Sun D, Hurley LH (2006) Deconvoluting the structural and drug-recognition complexity of the G-quadruplex-forming region upstream of the bcl-2 P1 promoter. J Am Chem Soc 128:5404–5415

6. Rankin S, Reszka AP, Huppert J, Zloh M, Parkinson GN et al (2005) Putative DNA quadruplex formation within the human c-kit oncogene. J Am Chem Soc 127:10584–10589
7. Simonsson T, Pecinka P, Kubista M (1998) DNA tetraplex formation in the control region of c-myc. Nucleic Acids Res 26:1167–1172
8. Sen D, Gilbert W (1988) Formation of parallel four-stranded complexes by guanine-rich motifs in DNA and its implications for meiosis. Nature 334:364–366
9. Hanakahi LA, Sun H, Maizels N (1999) High affinity interactions of nucleolin with G–G-paired rDNA. J Biol Chem 274: 15908–15912
10. Harrison RJ, Cuesta J, Chessari G, Read MA, Basra SK et al (2003) Trisubstituted acridine derivatives as potent and selective telomerase inhibitors. J Med Chem 46:4463–4476
11. Tan JH, Ou TM, Hou JQ, Lu YJ, Huang SL et al (2009) Isaindigotone derivatives: a new class of highly selective ligands for telomeric G-quadruplex DNA. J Med Chem 52:2825–2835
12. Oganesian L, Bryan TM (2007) Physiological relevance of telomeric G-quadruplex formation: a potential drug target. BioEssays 29:155–165
13. Paeschke K, Simonsson T, Postberg J, Rhodes D, Lipps HJ (2005) Telomere end-binding proteins control the formation of G-quadruplex DNA structures in vivo. Nat Struct Mol Biol 12:847–854
14. Duquette ML, Handa P, Vincent JA, Taylor AF, Maizels N (2004) Intracellular transcription of G-rich DNAs induces formation of G-loops, novel structures containing G4 DNA. Genes Dev 18:1618–1629
15. Baumann P, Cech TR (2001) Pot1, the putative telomere end-binding protein in fission yeast and humans. Science 292: 1171–1175
16. Dexheimer TS, Carey SS, Zuohe S, Gokhale VM, Hu X et al (2009) NM23-H2 may play an indirect role in transcriptional activation of c-myc gene expression but does not cleave the nuclease hypersensitive element III1. Mol Cancer Ther 8: 1363–1377
17. Haider SM, Parkinson GN, Neidle S (2003) Structure of a G-quadruplex-ligand complex. J Mol Biol 326:117–125
18. Campbell NH, Parkinson GN, Reszka AP, Neidle S (2008) Structural basis of DNA quadruplex recognition by an acridine drug. J Am Chem Soc 130:6722–6724
19. Clark GR, Pytel PD, Squire CJ, Neidle S (2003) Structure of the first parallel DNA quadruplex-drug complex. J Am Chem Soc 125:4066–4067
20. Gavathiotis E, Heald RA, Stevens MF, Searle MS (2003) Drug recognition and stabilisation of the parallel-stranded DNA quadruplex d(TTAGGGT)4 containing the human telomeric repeat. J Mol Biol 334:25–36
21. Hounsou C, Guittat L, Monchaud D, Jourdan M, Saettel N et al (2007) G-Quadruplex Recognition by Quinacridines: a SAR, NMR, and Biological Study. ChemMedChem 2:655–666
22. Phan AT, Kuryavyi V, Gaw HY, Patel DJ (2005) Small-molecule interaction with a five-guanine-tract G-quadruplex structure from the human MYC promoter. Nat Chem Biol 1:167–173
23. Neidle S (2009) The structures of quadruplex nucleic acids and their drug complexes. Curr Opin Struct Biol 19:239–250
24. Neidle S, Parkinson GN (2008) Quadruplex DNA crystal structures and drug design. Biochimie 90:1184–1196
25. Parkinson GN, Ghosh R, Neidle S (2007) Structural basis for binding of porphyrin to human telomeres. Biochemistry 46:2390–2397
26. Parkinson GN, Cuenca F, Neidle S (2008) Topology conservation and loop flexibility in quadruplex-drug recognition: crystal structures of inter- and intramolecular telomeric DNA quadruplex-drug complexes. J Mol Biol 381:1145–1156
27. Yang D, Okamoto K (2010) Structural insights into G-quadruplexes: towards new anticancer drugs. Future Med Chem 2:619–646
28. Padmanabhan K, Padmanabhan KP, Ferrara JD, Sadler JE, Tulinsky A (1993) The structure of alpha-thrombin inhibited by a 15-mer single-stranded DNA aptamer. J Biol Chem 268:17651–17654
29. Schonhoft JD, Das A, Achamyeleh F, Samdani S, Sewell A et al (2009) ILPR repeats adopt diverse G-quadruplex conformations that determine insulin binding. Biopolymers 93:21–31
30. Rodriguez D, Pineiro A, Gutierrez-de-Teran H (2011) Molecular dynamics simulations reveal insights into key structural elements of adenosine receptors. Biochemistry 50:4194–4208
31. Moore MJ, Schultes CM, Cuesta J, Cuenca F, Gunaratnam M et al (2006) Trisubstituted acridines as G-quadruplex telomere targeting agents. Effects of extensions of the 3,6- and 9-side chains on quadruplex binding, telomerase activity, and cell proliferation. J Med Chem 49:582–599
32. Cheatham TE 3rd (2004) Simulation and modeling of nucleic acid structure, dynamics and interactions. Curr Opin Struct Biol 14:360–367
33. Chowdhury S, Bansal M (2001) G-quadruplex structure can be stable with only some coordination sites being occupied by cations: a six-nanosecond molecular dynamics study. J Phys Chem B 105:7572–7578
34. Spackova N, Berger I, Sponer J (2001) Structural dynamics and cation interactions of DNA quadruplex molecules containing mixed guanine/cytosine quartets revealed by large-scale MD simulations. J Am Chem Soc 123:3295–3307
35. Fadrna E, Spackova N, Stefl R, Koca J, Cheatham TE 3rd et al (2004) Molecular dynamics simulations of guanine quadruplex loops: advances and force field limitations. Biophys J 87:227–242
36. Sponer J, Spackova N (2007) Molecular dynamics simulations and their application to four-stranded DNA. Methods 43:278–290
37. Haider S, Parkinson GN, Neidle S (2008) Molecular dynamics and principal components analysis of human telomeric quadruplex multimers. Biophys J 95:296–311
38. Yang DY, Chang TC, Sheu SY (2007) Interaction between human telomere and a carbazole derivative: a molecular dynamics simulation of a quadruplex stabilizer and telomerase inhibitor. J Phys Chem A 111:9224–9232
39. Agrawal S, Ojha RP, Maiti S (2008) Energetics of the human Tel-22 quadruplex-telomestatin interaction: a molecular dynamics study. J Phys Chem B 112:6828–6836
40. Cavallari M, Garbesi A, Di Felice R (2009) Porphyrin intercalation in G4-DNA quadruplexes by molecular dynamics simulations. J Phys Chem B 113:13152–13160
41. Frisch, MJT, Trucks GW, Schlegel HB, Scuseria GE, Robb MA et al. (2004) Gaussian 03, Revision E.01; Gaussian, Inc, Wallingford, CT
42. Case DA, Cheatham TE 3rd, Darden T, Gohlke H, Luo R et al (2005) The Amber biomolecular simulation programs. J Comput Chem 26:1668–1688
43. Wang J, Wolf RM, Caldwell JW, Kollman PA, Case DA (2004) Development and testing of a general amber force field. J Comput Chem 25:1157–1174
44. Cornell WD, Cieplak P, Bayly CI, Gould IR Jr, Ferguson DM et al (1995) A second generation force field for the simulation of proteins, nucleic acids, and organic molecules. J Am Chem Soc 117:5179
45. Ryckaert JP, Ciccotti G, Berendsen HJC (1977) Numerical integration of the Cartesian equations of motion of a system with constraints: molecular dynamics of n-alkanes. J Comput Phys 23:327–341
46. Darden T, York D, Pedersen L (1993) Particle mesh Ewald: an N log(N) method for Ewald sums in large systems. J Chem Phys 98:10089–10092

47. Humphrey W, Dalke A, Schulten K (1996) VMD: visual molecular dynamics. J Mol Graph 14(33–38):27–28
48. Kollman PA, Massova I, Reyes C, Kuhn B, Huo S et al (2000) Calculating structures and free energies of complex molecules: combining molecular mechanics and continuum models. Acc Chem Res 33:889–897
49. Fogolari F, Brigo A, Molinari H (2003) Protocol for MM/PBSA molecular dynamics simulations of proteins. Biophys J 85:159–166
50. Hazel P, Parkinson GN, Neidle S (2006) Predictive modelling of topology and loop variations in dimeric DNA quadruplex structures. Nucleic Acids Res 34:2117–2127
51. Zeng J, Li W, Zhao Y, Liu G, Tang Y et al (2008) Insights into ligand selectivity in estrogen receptor isoforms: molecular dynamics simulations and binding free energy calculations. J Phys Chem B 112:2719–2726
52. Gilson MK, Sharp KA, Honig B (1987) Calculating electrostatic interactions in biomolecules: method and error assessment. J Comput Chem 9:327–335
53. Still WC, Tempczyk A, Hawley RC, Hendrickson T (1990) Semianalytical treatment of solvation for molecular mechanics and dynamics. J Am Chem Soc 112:6127–6129
54. Pettersen EF, Goddard TD, Huang CC, Couch GS, Greenblatt DM et al (2004) UCSF Chimera—a visualization system for exploratory research and analysis. J Comput Chem 25:1605–1612
55. Amadei A, Linssen AB, Berendsen HJ (1993) Essential dynamics of proteins. Proteins 17:412–425
56. Amadei A, Linssen AB, de Groot BL, van Aalten DM, Berendsen HJ (1996) An efficient method for sampling the essential subspace of proteins. J Biomol Struct Dyn 13:615–625
57. Meyer T, Ferrer-Costa C, Perez A, Rueda M, Bidon-Chanal A et al (2006) Essential dynamics: a tool for efficient trajectory compression and management. J Chem Theory Comput 2: 251–258
58. DeLano WL (2002) The PyMOL molecular graphics system. DeLano Scientific, San Carlos, CA
59. Podbevsek P, Hud NV, Plavec J (2007) NMR evaluation of ammonium ion movement within a unimolecular G-quadruplex in solution. Nucleic Acids Res 35:2554–2563
60. Podbevsek P, Sket P, Plavec J (2008) Stacking and not solely topology of T3 loops controls rigidity and ammonium ion movement within d(G4T3G4)2 G-quadruplex. J Am Chem Soc 130:14287–14293
61. Sket P, Plavec J (2010) Tetramolecular DNA Quadruplexes in solution: insights into structural diversity and cation movement. J Am Chem Soc 132:12724–12732
62. Hou JQ, Chen SB, Tan JH, Ou TM, Luo HB et al (2010) New insights into the structures of ligand-quadruplex complexes from molecular dynamics simulations. J Phys Chem B 114:15301–15310
63. Zavasnik J, Podbevsek P, Plavec J (2011) Observation of water molecules within the bimolecular d(G3CT4G3C)2 G-quadruplex. Biochemistry 50:4155–4161
64. Miller MC, Buscaglia R, Chaires JB, Lane AN, Trent JO (2010) Hydration is a major determinant of the G-quadruplex stability and conformation of the human telomere 3′ sequence of d(AG3(TTAG3)3). J Am Chem Soc 132:17105–17107
65. Fan HY, Shek YL, Amiri A, Dubins DN, Heerklotz H et al (2011) Volumetric characterization of sodium-induced G-quadruplex formation. J Am Chem Soc 133:4518–4526
66. Stefl R, Spackova N, Berger I, Koca J, Sponer J (2001) Molecular dynamics of DNA quadruplex molecules containing inosine, 6-thioguanine and 6-thiopurine. Biophys J 80:455–468
67. Stefl R, Cheatham TE 3rd, Spackova N, Fadrna E, Berger I et al (2003) Formation pathways of a guanine-quadruplex DNA revealed by molecular dynamics and thermodynamic analysis of the substates. Biophys J 85:1787–1804
68. Cang X, Sponer J, Cheatham TE 3rd (2011) Explaining the varied glycosidic conformational, G-tract length and sequence preferences for anti-parallel G-quadruplexes. Nucleic Acids Res 39:4499–4512
69. Yue DJ, Lim KW, Phan AT (2011) Formation of (3 + 1) G-quadruplexes with a long loop by human telomeric DNA spanning five or more repeats. J Am Chem Soc 133:11462–11465
70. Collie GW, Promontorio R, Hampel SM, Micco M, Neidle S, Parkinson GN (2012) Structural basis for telomeric G-quadruplex targeting by naphthalene diimide ligands. J Am Chem Soc 134: 2723